

Spin polarization as a probe of the QCD critical point

De-Xian Wei¹

¹*School of Science, Guangxi University of Science and Technology, Liuzhou, 545006, China*

Spin polarization is a novel method for probing the rotational properties of the quark-gluon plasma (QGP) produced in relativistic heavy-ion collisions. In this work, we investigate the effective transport and thermodynamic coefficients in non-central O+O light-ion collisions, considering a parton distribution function that incorporates the spin polarization induced by thermal vorticity during the collision. Using a kinetic theory approach, we find that while the speed of sound squared (c_s^2) remains largely unaffected by spin polarization, the specific shear viscosity (η/s), specific bulk viscosity (ζ/s), and mean free path (λ) are significantly modified.

Notably, when spin polarization is taken into account, both c_s^2 and ζ/s exhibit a non-monotonic dependence on collision energy, with an inflection point around $\sqrt{s_{NN}} = 27$ GeV, corresponding to an average parton chemical potential of $\langle\mu_p\rangle = 0.021$ GeV. This non-monotonic behavior suggests that incorporating spin polarization into theoretical calculations could provide an effective probe for locating the critical point of the QCD phase transition.

Introduction - The study of the properties of nuclear matter governed by Quantum Chromodynamics (QCD) is a central topic in high-energy physics. To explore the rich phase structure of QCD in the finite-temperature and baryon chemical potential plane, extensive experimental efforts have been carried out through relativistic heavy-ion collisions, notably at the Relativistic Heavy Ion Collider (RHIC) and the Large Hadron Collider (LHC).

One of the open questions in QGP physics is whether the QCD phase diagram contains a critical endpoint (CEP) that separates a crossover transition at low baryon density from a conjectured first-order phase transition at high baryon chemical potential μ_B [1, 2]. During the past two decades, both theoretical and experimental investigations have made significant progress in mapping the QCD phase diagram [3], with particular focus on determining the possible location of the CEP in the phase space [4–13] (see also reviews [14, 15]).

Traditional numerical techniques face severe challenges in locating the CEP due to the sign problem in lattice QCD simulations at finite μ_B [16]. However, recently, first-principles studies based on extrinsic methods have suggested the presence of a critical point in a relatively narrow region of the QCD phase diagram, with estimates around $T_c \sim 0.100$ - 0.110 GeV and $\mu_c \sim 0.420$ - 0.650 GeV [11, 12, 17–19].

The Beam Energy Scan (BES) program at RHIC explores this possibility by colliding heavy nuclei over a wide range of center of mass energies, $\sqrt{s_{NN}} = 3$ - 200 GeV, to probe the CEP and study the equation of state of nuclear matter at high baryon densities, employing higher order cumulants of conserved charges and the yield ratios of light nuclei [13, 20–24].

Despite all these efforts, conclusive evidence for the existence or precise location of CEP remains elusive due to current experimental uncertainties [25].

However, recent experimental and theoretical studies have shown that spin polarization (SP) opens a new av-

enue of research [26–34] (see also reviews [35–38]). The strong vorticity produced in noncentral heavy-ion collisions can polarize hyperons, as confirmed by measurements at RHIC [39–42] and LHC [43, 44].

SP has been used to investigate the critical point of QCD [45, 46], due to its sensitivity to the transport coefficients of the quark-gluon plasma (QGP) [34, 47]. Moreover, the strong vorticity and magnetic fields generated in noncentral collisions can themselves influence the QGP transport coefficients [48–50].

These findings suggest that the SP encodes information about the time-dependent transport and thermodynamic properties of the QGP. Specifically, because SP is responsive to changes in these properties, it may serve as a valuable probe of the QCD phase transition.

Therefore, the primary objectives of this letter are as follows: for noncentral O+O light-ion collisions, (i) to investigate the impact of parton spin polarization on the effective transport and thermodynamic coefficients (TTC), and (ii) to explore the behavior of the QCD critical point by leveraging the sensitivity of SP. The choice of O+O collisions is motivated by their ability to generate vorticity while potentially undergoing a phase transition from hadronic matter to the QGP.

Spin polarization in kinetic theory - We began with the near-equilibrium, spin-dependent phase-space distribution function, parameterized as [30, 51, 52]:

$$\begin{aligned} & \tilde{f}_{rs}[r(\tau), p(\tau), s(\tau)] \\ &= f[r(\tau), p(\tau)] \times [\delta_{rs} + \Pi[r(\tau), p(\tau)]\sigma_{rs}]. \end{aligned} \quad (1)$$

Here, $f[r(\tau), p(\tau)]$ is the spinless distribution function, $s(\tau)$ denotes the spin degree of freedom in the phase-space distribution, σ_{rs} is a three-vector composed of the Pauli matrices, and $\Pi[r(\tau), p(\tau)]$ represents the spin-polarization three-vector. Under the assumption of small vorticity within the local thermodynamic equilibrium, a linear relationship arises between the averaged spin polarization vector and the thermal vorticity. Specifically, for spin-1/2 particles, the polarization vector satisfies

$\Pi^\mu \approx \varpi^\mu [2s(s+1)/3]$. A similar relation between Π^μ and ϖ^μ is discussed in [51, 53]. For spin polarization studies, it is convenient to express thermal vorticity in terms of a tensor: $\varpi^{\rho\sigma} = 1/2(\partial_\sigma\beta_\rho - \partial_\rho\beta_\sigma)$, and the thermal vorticity vector is given by $\varpi^\mu = 1/2\epsilon^{\mu\rho\sigma\tau}u_\rho\partial_\sigma\beta_\tau = -1/2\epsilon^{\mu\rho\sigma\tau}\varpi^{\rho\sigma}u_\tau$, where $\beta_\rho = u_\rho/T$, with u_ρ denoting the four-velocity of the fluid and T the temperature.

To highlight the contribution of spin polarization, we employed kinetic theory to calculate the energy-momentum tensor. Taking into account the spin measure, the SP-dependent energy-momentum tensor is defined as:

$$\begin{aligned}\tilde{T}^{\mu\nu}(\tau, r) &= \int \frac{d^3p}{(2\pi)^3} \frac{p^\mu p^\nu}{p^0} \int dS \tilde{f}[r(\tau), p(\tau), s(\tau)] \\ &= \int \frac{d^3p}{(2\pi)^3} \frac{p^\mu p^\nu}{p^0} f[r(\tau), p(\tau)] \\ &\times \int [\delta_{rs} + \Pi[r(\tau), p(\tau)]\sigma_{rs}] dS.\end{aligned}\quad (2)$$

Here, the invariant spin measure can be parameterized as [54]:

$$\begin{aligned}&\int [\delta_{rs} + \Pi[r(\tau), p(\tau)]\sigma_{rs}] dS \\ &\approx 1 - \frac{2 \sinh[\chi \Pi[r(\tau), p(\tau)]]}{\chi \Pi[r(\tau), p(\tau)]},\end{aligned}\quad (3)$$

where $\chi^2 = 3/4$. We do not distinguish between particles and antiparticles because the chemical potential is not introduced in this framework. The distribution function sums over the spin-up and spin-down quarks and anti-quarks. For comparison, the spinless energy-momentum tensor is given by:

$$T^{\mu\nu}(\tau, r) = \int \frac{d^3p}{(2\pi)^3} \frac{p^\mu p^\nu}{p^0} f[r(\tau), p(\tau)].\quad (4)$$

The factor $d^3p/(2\pi)^3/p^0$ is the Lorentz invariant integration measure in momentum space, where $p^0 = \sqrt{m^2 + p^2}$ is the on-shell energy of the particle.

By evaluating the energy-momentum tensor, one can extract the TTCs, such as the specific shear viscosity η/s , the specific bulk viscosity ζ/s , and the mean free path λ , which are of central interest in QGP physics. The first-order, spinless TTCs for massive particles in kinetic theory are defined as:

$$\begin{aligned}\eta/s &= \frac{1}{15(\varepsilon + P)} \int \frac{d^3p}{(2\pi)^3} \frac{p^4}{p^0} f(1-f) \\ \zeta/s &= 15\eta/s \left(\frac{1}{3} - c_s^2 \right) \\ &= \frac{1}{(\varepsilon + P)} \left(\frac{1}{3} - c_s^2 \right) \int \frac{d^3p}{(2\pi)^3} \frac{p^4}{p^0} f(1-f) \\ \lambda &\approx \frac{5}{T} \eta/s \\ &= \frac{1}{3(\varepsilon + P)T} \int \frac{d^3p}{(2\pi)^3} \frac{p^4}{p^0} f(1-f).\end{aligned}\quad (5)$$

Here, the local temperature is defined as $T = \langle p_T \rangle / 3$, where p_T denotes the transverse momentum of the particle. The energy density and pressure are obtained from Eq. (4), specifically: $\varepsilon = T^{00}$, $P = \sqrt{T^{11} + T^{22} + T^{33}}$. The squared speed of sound is defined as the derivative of the pressure with respect to the energy density at constant entropy: $c_s^2 = (\partial P / \partial \varepsilon)_s$.

Similarly, the first-order spin-polarization-dependent TTC for massive particles are defined as:

$$\begin{aligned}\tilde{\eta}/\tilde{s} &= \frac{1}{15(\tilde{\varepsilon} + \tilde{P})} \int \frac{d^3p}{(2\pi)^3} \frac{p^4}{p^0} dS \tilde{f}(1-\tilde{f}) \\ \tilde{\zeta}/\tilde{s} &= \frac{1}{(\tilde{\varepsilon} + \tilde{P})} \left(\frac{1}{3} - \tilde{c}_s^2 \right) \int \frac{d^3p}{(2\pi)^3} \frac{p^4}{p^0} dS \tilde{f}(1-\tilde{f}) \\ \tilde{\lambda} &\approx \frac{1}{3(\tilde{\varepsilon} + \tilde{P})T} \int \frac{d^3p}{(2\pi)^3} \frac{p^4}{p^0} dS \tilde{f}(1-\tilde{f}),\end{aligned}\quad (6)$$

where $\tilde{\varepsilon} = \tilde{T}^{00}$, $\tilde{P} = \sqrt{\tilde{T}^{11} + \tilde{T}^{22} + \tilde{T}^{33}}$, and $\tilde{c}_s^2 = (\partial \tilde{P} / \partial \tilde{\varepsilon})_s$. Both the vorticity tensor and the viscosity coefficients are dissipative quantities related to the relaxation time.

In this work, the TTC are investigated in O+O collisions with an impact parameter $b = 3$ fm, using the A Multi-Phase Transport (AMPT) model [55]. We do not apply a multiplicity filter; instead, we fix the impact parameter, which results in a wide range of multiplicities, from low to high values.

This letter uses the default collision probability parameters in AMPT: $a = 0.5$, $b = 0.9 \text{ GeV}^{-2}$, $\alpha_s = 0.33$ and $\mu = 3.2 \text{ fm}^{-1}$. The AMPT model includes the transport processes that simulate parton interactions, and incorporates a natural viscosity that depends on the scattering cross section, as formulated in the Israel-Stewart or Chapman-Enskog frameworks [56, 57].

At the critical endpoint of QCD, the correlation length diverges [58], leading to divergences in several thermodynamic quantities, which may affect observables related to QGP. The probability of observing such effects increases if the freeze-out curve in the $\mu - T$ plane passes sufficiently close to the CEP.

To study the impact of spin polarization on transport and thermodynamic properties, we reextract the TTC using the kinetic theory framework, as defined in Eqs. (5)–(6). We consider spin polarization only during the partonic stage and assume that it is generated solely by thermal vorticity arising from angular momentum, neglecting other sources such as magnetic fields, thermal shear, or viscous effects.

Throughout this work, we adopt natural units with $k_B = c = \hbar = 1$.

Numerical results - After introducing the kinetic theory framework above, we now present numerical results for the transport and thermodynamic coefficients (TTC). A more detailed numerical analysis will be reported in a follow-up study.

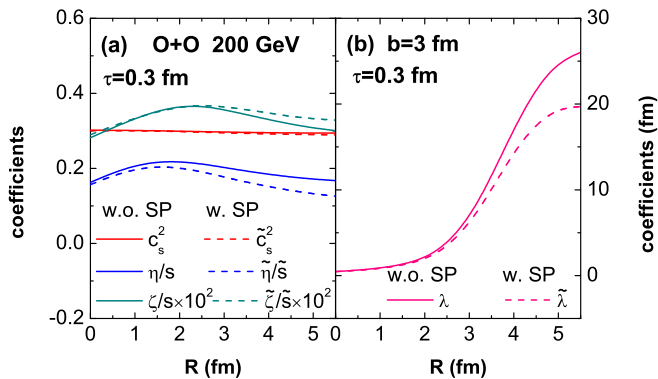


FIG. 1. (Color online) Comparison between SP and non-SP results: (a) the speed of sound squared c_s^2 , specific shear viscosity η/s , and specific bulk viscosity ζ/s ; (b) the mean free path λ , shown as functions of radius for O+O collisions at 200 GeV. The results correspond to a proper time $\tau = 0.3$ fm.

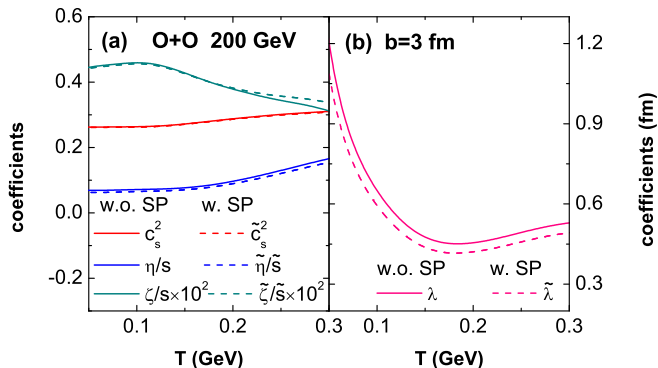


FIG. 2. (Color online) Comparison between SP and non-SP results: (a) c_s^2 , η/s , and ζ/s ; (b) λ shown as functions of temperature for O+O collisions at 200 GeV. The results are integrated over proper time from $\tau = 0$ to 5 fm.

Figure 1 presents the speed of sound squared c_s^2 , the specific shear viscosity η/s , the specific bulk viscosity ζ/s , and the mean free path λ as functions of radius for O+O collisions at 200 GeV, evaluated at proper time $\tau = 0.3$ fm. Among these, all coefficients except c_s^2 show significant sensitivity to spin polarization.

Vorticity defines a noninertial reference frame in which physical quantities receive noninertial corrections. This implies that spin polarization, as a non-dissipative effect, modifies the transport properties of the system when viewed in such a frame [51]. In Fig. 1, the splitting between SP and non-SP results increases with radius, which is attributed to the thermal vorticity exhibiting a quadrupole distribution in the coordinate space [28]. In other words, the effect of spin polarization on the TTC is volume dependent.

Interestingly, SP has opposite effects on specific shear and bulk viscosities. Shear viscosity reflects momentum transport, primarily influenced by Coriolis forces under

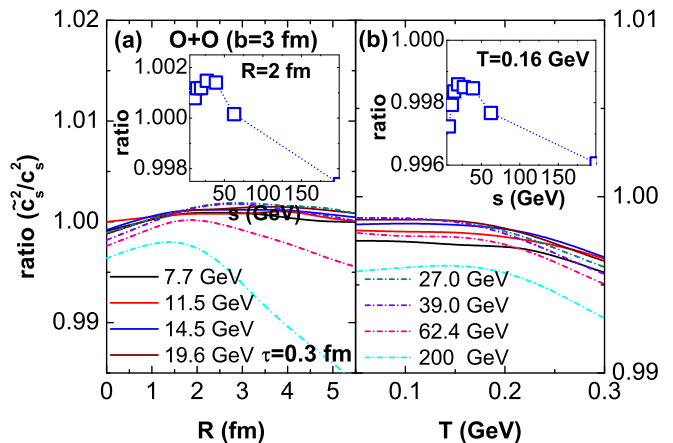


FIG. 3. (Color online) Left panel: The ratio \tilde{c}_s^2/c_s^2 as a function of radius, shown at proper time $\tau = 0.3$ fm. Right panel: The same ratio as a function of temperature, integrated over proper time from $\tau = 0$ to 5 fm. Simulated results correspond to O+O collisions at $\sqrt{s_{NN}} = 7.7$ –200 GeV.

finite rotation [48], while the bulk viscosity describes pressure changes due to the expansion or compression of the local fluid. As a result, the SP contributions to these two coefficients behave differently.

The mean free path λ is calculated directly from η/s , and its behavior qualitatively mirrors that of η/s . It is important to note that the results presented here correspond to the very early stage of the system evolution, where the coefficients are most strongly affected.

Time-dependent splitting effects are provided in the supplementary material and are consistent with previous findings [59].

In Fig. 2, the values of c_s^2 , η/s , ζ/s , and λ are shown as functions of temperature for O+O collisions at 200 GeV, integrated over the proper time from $\tau = 0$ to 5 fm. Similar to the radius-dependent behavior observed in Fig. 1, all coefficients are significantly affected by spin polarization (SP), except for the speed of sound squared c_s^2 , which shows only a weak dependence.

Across the temperature range, the contribution of SP to η/s demonstrates a general suppression. In contrast, the effect of SP on ζ/s shows a sign reversal: it suppresses ζ/s at lower temperatures but enhances it at higher temperatures, with a crossover point near $T \sim 0.16$ GeV. A similar, though weaker, sign-reversal behavior is also observed in c_s^2 . These findings suggest that the phase transition properties of nuclear matter can be inferred from the response of c_s^2 and ζ/s to SP. As with η/s , the SP contribution to λ also exhibits suppression. Note that the calculation of λ is directly linked to η/s .

To investigate the characteristics of the QCD critical point, the ratio \tilde{c}_s^2/c_s^2 is calculated for different collision energies, as shown in Fig. 3. In Fig. 3(a), the ratio is plotted as a function of radius at $\tau = 0.3$ fm. Interestingly,

the radial behavior exhibits a nonmonotonic dependence on collision energy, with a peak around 27 GeV (specifically at radius $R = 2$ fm). As the radius increases, SP increases because of the increased orbital angular momentum, causing the critical signal to shift away from the center. This is consistent with previous model calculations [46, 60].

Although separating spin from total angular momentum remains challenging, the present analysis qualitatively reveals the influence of finite volume and vorticity on the QCD phase structure, thereby explaining the observed nonmonotonic behavior.

In Fig. 3(b), the ratio \tilde{c}_s^2/c_s^2 is plotted as a function of temperature, again showing a nonmonotonic dependence on energy, with a peak near 19.6 GeV (i.e., $T \approx 0.16$ GeV). This behavior is consistent with experimental observations at RHIC, particularly in high-order cumulants of net protons, scaling exponents, and yield ratios of light nuclei [21–24].

The nonmonotonic energy dependence suggests that the dense matter produced in these collisions may pass through the critical region, experiencing critical fluctuations—an important signal in the search for the QCD critical point [13, 61, 62].

It should be noted that spin polarization characterizes a nondissipative quantity in thermodynamic equilibrium, while specific viscosities are dissipative quantities relevant to the nonequilibrium evolution of the system. Therefore, the contribution of SP to the viscosity coefficients may reflect scale invariance associated with the phase transition.

Although functional Renormalization Group (fRG) and Dyson-Schwinger Equation (DSE) studies predict that the CEP lies at $\mu_c \gtrsim 420$ MeV [11, 12, 17–19], corresponding to collision energies around 7.7 GeV, the behavior in the lower energy region ($\lesssim 7.7$ GeV) may involve a first-order phase transition or no formation of a QGP at all.

It is also important to note that many theoretical models assume local thermal equilibrium when describing critical fluctuations. However, non-equilibrium effects can play a crucial role in heavy-ion collisions [63]. Additional support for these non-equilibrium effects is provided in the supplementary material.

Moreover, nonmonotonic behavior is not unique to critical fluctuations. Calculations using the Nambu–Jona-Lasinio (NJL) and Polyakov–Nambu–Jona-Lasinio (PNJL) models show that the nonmonotonic behavior of the $\kappa\sigma^2 - \sqrt{s_{NN}}$ curve is not due solely to the CEP [5, 64]. Instead, it may arise from the continuous sharpening of the chiral crossover, which increases the correlation length [9].

To further validate the conclusions drawn from Fig. 3, we present the $R - \sqrt{s_{NN}}$ and $T - \sqrt{s_{NN}}$ distributions of the ratios $(\tilde{\eta}/\tilde{s})/(\eta/s)$, $(\tilde{\zeta}/\tilde{s})/(\zeta/s)$ and $\tilde{\lambda}/\lambda$ in Fig. 4. The top panels of Fig. 4 show the $R - \sqrt{s_{NN}}$ distributions

of these transport coefficient ratios, comparing the results from the SP and non-SP methods. At a specific radius $R = 2$ fm, the ratios $(\tilde{\eta}/\tilde{s})/(\eta/s)$, and $\tilde{\lambda}/\lambda$ decrease monotonically with increasing collision energy, whereas the ratio $(\tilde{\zeta}/\tilde{s})/(\zeta/s)$ exhibits a nonmonotonic dependence. This nonmonotonicity is influenced by the behavior of the speed of sound squared c_s^2 , which contributes to the reversed trend seen in the ratio \tilde{c}_s^2/c_s^2 .

The bottom panels of Fig. 4 present the $T - \sqrt{s_{NN}}$ distributions of the same coefficients, showing temperature-dependent behavior consistent with radius-dependent results. At the critical temperature $T = 0.16$ GeV, both $(\tilde{\eta}/\tilde{s})/(\eta/s)$ and $\tilde{\lambda}/\lambda$ decrease monotonically with increasing energy, while $(\tilde{\zeta}/\tilde{s})/(\zeta/s)$ again exhibits nonmonotonic behavior.

These observations are potentially driven by rapid fluctuations in order parameters near the critical region. The results suggest that vorticity effects are more pronounced near the QCD critical point than in regions farther from it, in agreement with predictions of the NJL model [65]. Therefore, the observed nonmonotonic behavior supports the possible existence of a first-order phase transition and a critical point near collision energies such as 27 GeV.

To investigate QCD properties at finite chemical potential, we introduce the averaged parton chemical potential, defined as

$$\langle \mu_p \rangle = \frac{\int \mu_p(\tau) d\tau}{\int d\tau} \quad (7)$$

where $\mu_p(\tau) = (T_c/2) \log[N_p(\tau)/N_{\bar{p}}(\tau)]$ is computed for a single collision event, following the approach in Ref. [66]. Here, the particle number is defined as $N_p(\tau) = N_u(\tau) + N_d(\tau) + N_s(\tau)$, and the antiparticle number as $N_{\bar{p}}(\tau) = N_{\bar{u}}(\tau) + N_{\bar{d}}(\tau) + N_{\bar{s}}(\tau)$, where the subscripts denote the quark flavors. The critical temperature is set to $T_c = 0.16$ GeV.

In Fig. 5(a), we extract the averaged parton chemical potential $\langle \mu_p \rangle$, which decreases monotonically with increasing collision energy. In Fig. 5(b), the ratios \tilde{c}_s^2/c_s^2 and $(\tilde{\zeta}/\tilde{s})/(\zeta/s)$, extracted from Fig. 3(b) and Fig. 4(b2), respectively, are shown as functions of $\langle \mu_p \rangle$, using the correspondence between $\sqrt{s_{NN}}$ and $\langle \mu_p \rangle$ established in Fig. 5(a).

The nonmonotonic behavior observed in these ratios constrains the inflection point to the range $\langle \mu_p \rangle \sim (0.017, 0.026)$ GeV, corresponding to the collision energies $\sqrt{s_{NN}} \sim (19.6, 39)$ GeV. We conclude that thermal vorticity-induced spin polarization significantly broadens the range of parton chemical potentials that are sensitive to critical point phenomena. Furthermore, the nonmonotonic features observed in Fig. 5(b) can be interpreted as a function of $\langle \mu_p \rangle$. Similar trends have been reported in [67] using hydrodynamic simulations combined with Bayesian analysis, although their study focuses on the chemical potential of baryons.

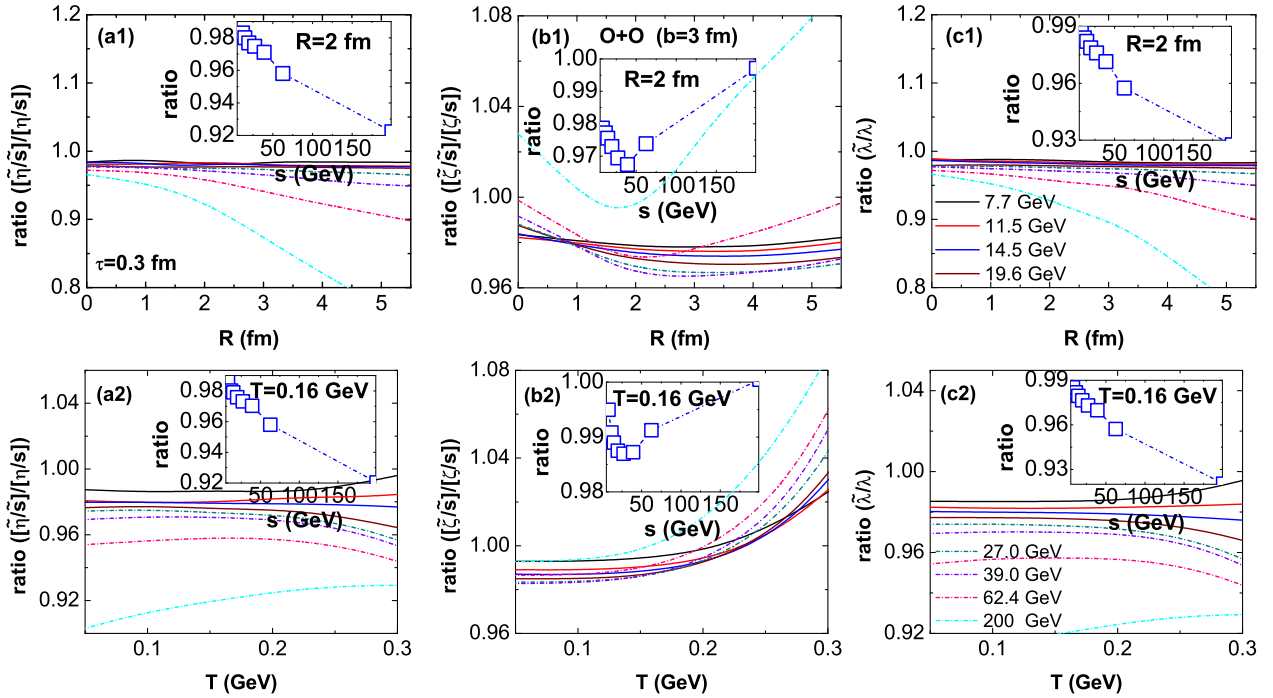


FIG. 4. (Color online) Top panels: Radial dependence of the ratios $(\tilde{\eta}/\bar{s})/(\eta/s)$, $(\tilde{\zeta}/\bar{s})/(\zeta/s)$ and $\tilde{\lambda}/\lambda$ for different collision energies in O+O collisions. Results are shown at proper time $\tau = 0.3$ fm. Bottom panels: Temperature dependence of the same ratios for different collision energies in O+O collisions. Results are integrated over proper time from $\tau = 0$ to 5 fm.

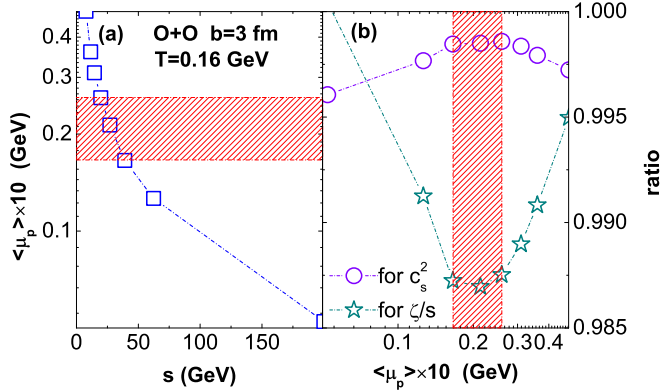


FIG. 5. (Color online) Left panel: Average parton chemical potential $\langle\mu_p\rangle$ as a function of collision energy. Right panel: Ratios \tilde{c}_s^2/c_s^2 and $(\tilde{\zeta}/\bar{s})/(\zeta/s)$ as functions of the average parton chemical potential $\langle\mu_p\rangle$.

Conclusions – We employed the A Multi-Phase Transport (AMPT) model to simulate the space-time evolution in non-central O+O collisions. Our results indicate that incorporating spin polarization (SP) into the model significantly influences the effective transport and thermodynamic coefficients (TTC) of partons. Additionally, based on these calculations, we observe a non-monotonic, energy-dependent behavior in the ratios \tilde{c}_s^2/c_s^2

and $(\tilde{\zeta}/\bar{s})/(\zeta/s)$. These trends suggest that SP may serve as an effective probe for identifying the critical point of the QCD phase transition.

We note that this study considers only the contribution of thermal vorticity to SP, while neglecting other potential sources such as thermal shear and magnetic fields. Furthermore, our approach employs kinetic theory without modeling the self-consistent evolution of the underlying microscopic dynamics. A more comprehensive model should incorporate these effects.

Despite these limitations, the non-monotonic behavior of the TTCs exhibits an inflection point around $\sqrt{s_{NN}} = 19.6\text{--}27$ GeV, helping to constrain the possible location of the critical point within the framework of our simplified model. Therefore, our findings may provide valuable guidance for future experiments in QGP physics.

This work is supported by NSFC through Grant No. 12105057, and Guangxi NSF through Grant No. 2023GXNSFAA026020, 2019GXNSFBA245080.

-
- [1] Z. Fodor and S. D. Katz, *JHEP* **04**, 050 (2004), [arXiv:hep-lat/0402006](https://arxiv.org/abs/hep-lat/0402006).
 [2] Y. Aoki, G. Endrodi, Z. Fodor, S. D. Katz, and K. K. Szabo, *Nature* **443**, 675 (2006), [arXiv:hep-lat/0611014](https://arxiv.org/abs/hep-lat/0611014).

- [3] W. Busza, K. Rajagopal, and W. van der Schee, *Ann. Rev. Nucl. Part. Sci.* **68**, 339 (2018), arXiv:1802.04801 [hep-ph].
- [4] X. Wang, M. Wei, Z. Li, and M. Huang, *Phys. Rev. D* **99**, 016018 (2019), arXiv:1808.01931 [hep-ph].
- [5] Z. Li, K. Xu, X. Wang, and M. Huang, *Eur. Phys. J. C* **79**, 245 (2019), arXiv:1801.09215 [hep-ph].
- [6] S. Borsányi, Z. Fodor, J. N. Guenther, R. Kara, S. D. Katz, P. Parotto, A. Pásztor, C. Ratti, and K. K. Szabó, *Phys. Rev. Lett.* **126**, 232001 (2021), arXiv:2102.06660 [hep-lat].
- [7] D. Bollweg, D. A. Clarke, J. Goswami, O. Kaczmarek, F. Karsch, S. Mukherjee, P. Petreczky, C. Schmidt, and S. Sharma (HotQCD), *Phys. Rev. D* **108**, 014510 (2023), arXiv:2212.09043 [hep-lat].
- [8] Y. Fujimoto, K. Fukushima, and Y. Hidaka, *Phys. Lett. B* **816**, 136184 (2021), arXiv:2101.09173 [hep-ph].
- [9] W.-j. Fu, X. Luo, J. M. Pawłowski, F. Rennecke, R. Wen, and S. Yin, *Phys. Rev. D* **104**, 094047 (2021), arXiv:2101.06035 [hep-ph].
- [10] Y. Lu, F. Gao, Y.-X. Liu, and J. M. Pawłowski, *Phys. Rev. D* **110**, 014036 (2024), arXiv:2310.18383 [hep-ph].
- [11] P. J. Gunkel and C. S. Fischer, *Phys. Rev. D* **104**, 054022 (2021), arXiv:2106.08356 [hep-ph].
- [12] M. Hippert, J. Grefa, T. A. Manning, J. Noronha, J. Noronha-Hostler, I. Portillo Vazquez, C. Ratti, R. Rougemont, and M. Trujillo, *Phys. Rev. D* **110**, 094006 (2024), arXiv:2309.00579 [nucl-th].
- [13] X. Luo and N. Xu, *Nucl. Sci. Tech.* **28**, 112 (2017), arXiv:1701.02105 [nucl-ex].
- [14] A. Bzdak, S. Esumi, V. Koch, J. Liao, M. Stephanov, and N. Xu, *Phys. Rept.* **853**, 1 (2020), arXiv:1906.00936 [nucl-th].
- [15] L. Du, A. Sorensen, and M. Stephanov, *Int. J. Mod. Phys. E* **33**, 2430008 (2024), arXiv:2402.10183 [nucl-th].
- [16] K. Nagata, *Prog. Part. Nucl. Phys.* **127**, 103991 (2022), arXiv:2108.12423 [hep-lat].
- [17] W.-j. Fu, J. M. Pawłowski, and F. Rennecke, *Phys. Rev. D* **101**, 054032 (2020), arXiv:1909.02991 [hep-ph].
- [18] F. Gao and J. M. Pawłowski, *Phys. Lett. B* **820**, 136584 (2021), arXiv:2010.13705 [hep-ph].
- [19] G. Basar, *Phys. Rev. C* **110**, 015203 (2024), arXiv:2312.06952 [hep-th].
- [20] K.-J. Sun, L.-W. Chen, C. M. Ko, J. Pu, and Z. Xu, *Phys. Lett. B* **781**, 499 (2018), arXiv:1801.09382 [nucl-th].
- [21] J. Adam *et al.* (STAR), *Phys. Rev. Lett.* **126**, 092301 (2021), arXiv:2001.02852 [nucl-ex].
- [22] M. S. Abdallah *et al.* (STAR), *Phys. Rev. Lett.* **128**, 202303 (2022), arXiv:2112.00240 [nucl-ex].
- [23] M. Abdallah *et al.* (STAR), *Phys. Rev. C* **107**, 024908 (2023), arXiv:2209.11940 [nucl-ex].
- [24] M. Abdulhamid *et al.* (STAR), *Phys. Rev. Lett.* **130**, 202301 (2023), arXiv:2209.08058 [nucl-ex].
- [25] A. Sorensen and P. Sorensen, (2024), arXiv:2405.10278 [nucl-th].
- [26] Z.-T. Liang and X.-N. Wang, *Phys. Rev. Lett.* **94**, 102301 (2005), [Erratum: *Phys. Rev. Lett.* **96**, 039901 (2006)], arXiv:nucl-th/0410079.
- [27] W. Florkowski, B. Friman, A. Jaiswal, and E. Speranza, *Phys. Rev. C* **97**, 041901 (2018), arXiv:1705.00587 [nucl-th].
- [28] D.-X. Wei, W.-T. Deng, and X.-G. Huang, *Phys. Rev. C* **99**, 014905 (2019), arXiv:1810.00151 [nucl-th].
- [29] K. Fukushima and S. Pu, *Phys. Lett. B* **817**, 136346 (2021), arXiv:2010.01608 [hep-th].
- [30] N. Weickgenannt, E. Speranza, X.-l. Sheng, Q. Wang, and D. H. Rischke, *Phys. Rev. Lett.* **127**, 052301 (2021), arXiv:2005.01506 [hep-ph].
- [31] S. Shi, C. Gale, and S. Jeon, *Phys. Rev. C* **103**, 044906 (2021), arXiv:2008.08618 [nucl-th].
- [32] W. Florkowski, R. Ryblewski, R. Singh, and G. Sophys, *Phys. Rev. D* **105**, 054007 (2022), arXiv:2112.01856 [hep-ph].
- [33] E. Speranza, F. S. Bemfica, M. M. Disconzi, and J. Noronha, *Phys. Rev. D* **107**, 054029 (2023), arXiv:2104.02110 [hep-th].
- [34] A. Palermo, E. Grossi, I. Karpenko, and F. Becattini, *Eur. Phys. J. C* **84**, 920 (2024), arXiv:2404.14295 [nucl-th].
- [35] F. Becattini and M. A. Lisa, *Ann. Rev. Nucl. Part. Sci.* **70**, 395 (2020), arXiv:2003.03640 [nucl-ex].
- [36] F. Becattini, *Rept. Prog. Phys.* **85**, 122301 (2022), arXiv:2204.01144 [nucl-th].
- [37] F. Becattini, M. Buzzegoli, T. Niida, S. Pu, A.-H. Tang, and Q. Wang, *Int. J. Mod. Phys. E* **33**, 2430006 (2024), arXiv:2402.04540 [nucl-th].
- [38] T. Niida and S. A. Voloshin, *Int. J. Mod. Phys. E* **33**, 2430010 (2024), arXiv:2404.11042 [nucl-ex].
- [39] L. Adamczyk *et al.* (STAR), *Nature* **548**, 62 (2017), arXiv:1701.06657 [nucl-ex].
- [40] J. Adam *et al.* (STAR), *Phys. Rev. Lett.* **123**, 132301 (2019), arXiv:1905.11917 [nucl-ex].
- [41] M. S. Abdallah *et al.* (STAR), *Phys. Rev. C* **104**, L061901 (2021), arXiv:2108.00044 [nucl-ex].
- [42] M. S. Abdallah *et al.* (STAR), *Nature* **614**, 244 (2023), arXiv:2204.02302 [hep-ph].
- [43] S. Acharya *et al.* (ALICE), *Phys. Rev. Lett.* **125**, 012301 (2020), arXiv:1910.14408 [nucl-ex].
- [44] S. Acharya *et al.* (ALICE), *Phys. Rev. Lett.* **128**, 172005 (2022), arXiv:2107.11183 [nucl-ex].
- [45] S. K. Singh and J.-e. Alam, *Eur. Phys. J. C* **83**, 585 (2023), arXiv:2110.15604 [hep-ph].
- [46] H.-L. Chen, W.-j. Fu, X.-G. Huang, and G.-L. Ma, (2024), arXiv:2410.20704 [hep-ph].
- [47] W. M. Serenone, J. a. G. P. Barbon, D. D. Chinellato, M. A. Lisa, C. Shen, J. Takahashi, and G. Torrieri, *Phys. Lett. B* **820**, 136500 (2021), arXiv:2102.11919 [hep-ph].
- [48] C. W. Aung, A. Dwibedi, J. Dey, and S. Ghosh, *Phys. Rev. C* **109**, 034913 (2024), arXiv:2303.16462 [nucl-th].
- [49] B. Sahoo, C. R. Singh, D. Sahu, R. Sahoo, and J.-e. Alam, *Eur. Phys. J. C* **83**, 873 (2023), arXiv:2302.07668 [hep-ph].
- [50] S. Rath and S. Dash, (2024), arXiv:2403.01240 [hep-ph].
- [51] F. Becattini, V. Chandra, L. Del Zanna, and E. Grossi, *Annals Phys.* **338**, 32 (2013), arXiv:1303.3431 [nucl-th].
- [52] W. Florkowski, A. Kumar, and R. Ryblewski, *Acta Phys. Polon. B* **51**, 945 (2020), arXiv:1907.09835 [nucl-th].
- [53] F. Becattini, I. Karpenko, M. Lisa, I. Upszal, and S. Voloshin, *Phys. Rev. C* **95**, 054902 (2017), arXiv:1610.02506 [nucl-th].
- [54] W. Florkowski, A. Kumar, and R. Ryblewski, *Prog. Part. Nucl. Phys.* **108**, 103709 (2019), arXiv:1811.04409 [nucl-th].
- [55] Z.-W. Lin, C. M. Ko, B.-A. Li, B. Zhang, and S. Pal, *Phys. Rev. C* **72**, 064901 (2005), arXiv:nucl-th/0411110.
- [56] N. M. MacKay and Z.-W. Lin, *Eur. Phys. J. C* **82**, 918 (2022), arXiv:2208.06027 [nucl-th].

- [57] Y. Zhang and Q. Liu, *Eur. Phys. J. A* **59**, 296 (2023).
- [58] M. A. Stephanov, K. Rajagopal, and E. V. Shuryak, *Phys. Rev. Lett.* **81**, 4816 (1998), [arXiv:hep-ph/9806219](#).
- [59] T. Nunes da Silva, D. Chinellato, M. Hippert, W. Serenone, J. Takahashi, G. S. Denicol, M. Luzum, and J. Noronha, *Phys. Rev. C* **103**, 054906 (2021), [arXiv:2006.02324 \[nucl-th\]](#).
- [60] H.-L. Chen, Z.-B. Zhu, and X.-G. Huang, *Phys. Rev. D* **108**, 054006 (2023), [arXiv:2306.08362 \[hep-ph\]](#).
- [61] D. Mroczek, A. R. Nava Acuna, J. Noronha-Hostler, P. Parotto, C. Ratti, and M. A. Stephanov, *Phys. Rev. C* **103**, 034901 (2021), [arXiv:2008.04022 \[nucl-th\]](#).
- [62] T. Dore, J. M. Karthein, I. Long, D. Mroczek, J. Noronha-Hostler, P. Parotto, C. Ratti, and Y. Yamauchi, *Phys. Rev. D* **106**, 094024 (2022), [arXiv:2207.04086 \[nucl-th\]](#).
- [63] M. Pradeep, K. Rajagopal, M. Stephanov, and Y. Yin, *Phys. Rev. D* **106**, 036017 (2022), [arXiv:2204.00639 \[hep-ph\]](#).
- [64] W. Fan, X. Luo, and H. Zong, *Chin. Phys. C* **43**, 033103 (2019), [arXiv:1702.08674 \[hep-ph\]](#).
- [65] Z. Zhang, C. Shi, X.-T. He, X. Luo, and H.-S. Zong, *Phys. Rev. D* **102**, 114023 (2020), [arXiv:2012.01017 \[hep-ph\]](#).
- [66] N. Yu, F. Liu, and K. Wu, *Phys. Rev. C* **90**, 024913 (2014), [arXiv:1404.5359 \[hep-ph\]](#).
- [67] C. Shen, B. Schenke, and W. Zhao, *Phys. Rev. Lett.* **132**, 072301 (2024), [arXiv:2310.10787 \[nucl-th\]](#).

Supplementary material

Figure S1 illustrates the transport and thermodynamic coefficients, including the specific shear viscosity η/s , specific bulk viscosity ζ/s , and mean free path λ , for O+O collisions at 200 GeV at different proper times. The differences between the SP and non-SP methods are most pronounced at early proper times and gradually diminish as the system evolves.

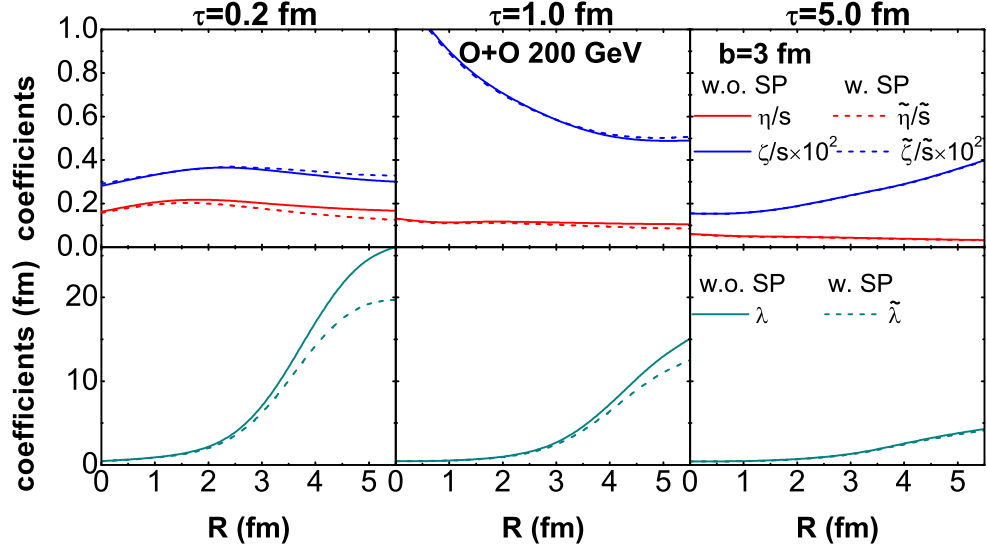


FIG. S1. (Color online) Comparison between the SP and non-SP method results. The transport and thermodynamic coefficients η/s , ζ/s and λ are shown as functions of radius for O+O collisions at 200 GeV. Results are presented at proper times $\tau = 0.2$, 1.0, and 5.0 fm, respectively.

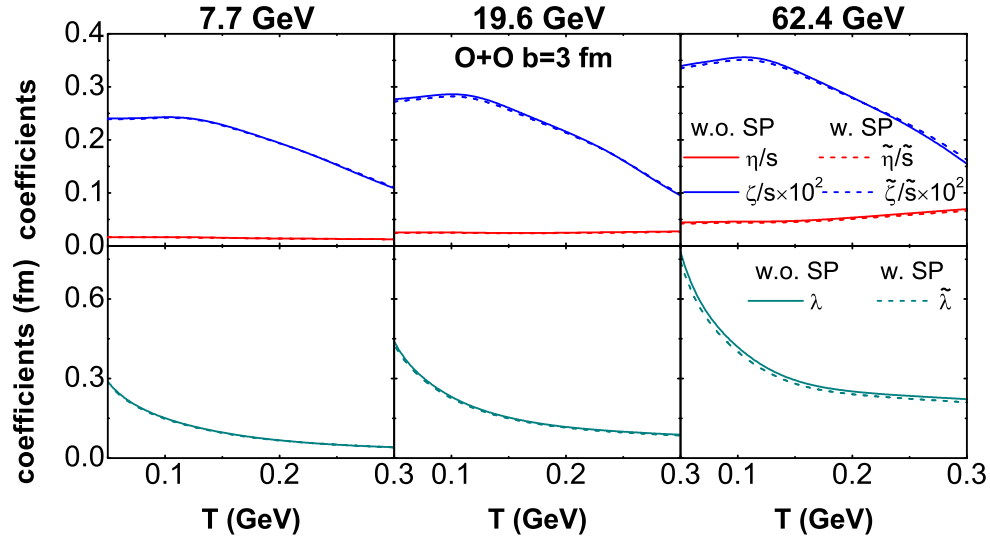


FIG. S2. (Color online) Comparison between the SP and non-SP method results. The transport and thermodynamic coefficients η/s , ζ/s , and λ are shown as functions of temperature for O+O collisions at $\sqrt{s_{NN}} = 7.7$, 19.6, and 62.4 GeV, respectively. Results are integrated over proper time from $\tau = 0$ to 5 fm.

Figure S2 presents the transport and thermodynamic coefficients, including the specific shear viscosity η/s , specific bulk viscosity ζ/s , and mean free path λ , for O+O collisions at $\sqrt{s_{NN}} = 7.7$, 19.6, and 62.4 GeV. The discrepancies between the SP and non-SP methods vary significantly across these different energies.